Supporting information

Industrial waste-derived nanoparticles and microspheres can be potent anti-microbial and functional ingredients

Manashi Das Purkayastha[a], Ajay Kumar Manhar[b], Manabendra Mandal[b], Charu Lata Mahanta[a]*

[a]Department of Food Engineering and Technology, School of Engineering, Tezpur University, Assam, India.

[b]Department of Molecular Biology and Biotechnology, School of Science, Tezpur University, Assam, India.

*Corresponding author: Charu Lata Mahanta

Department of Food Engineering and Technology, School of Engineering, Tezpur University, Assam, India -784028

e-mail address: charu@tezu.ernet.in

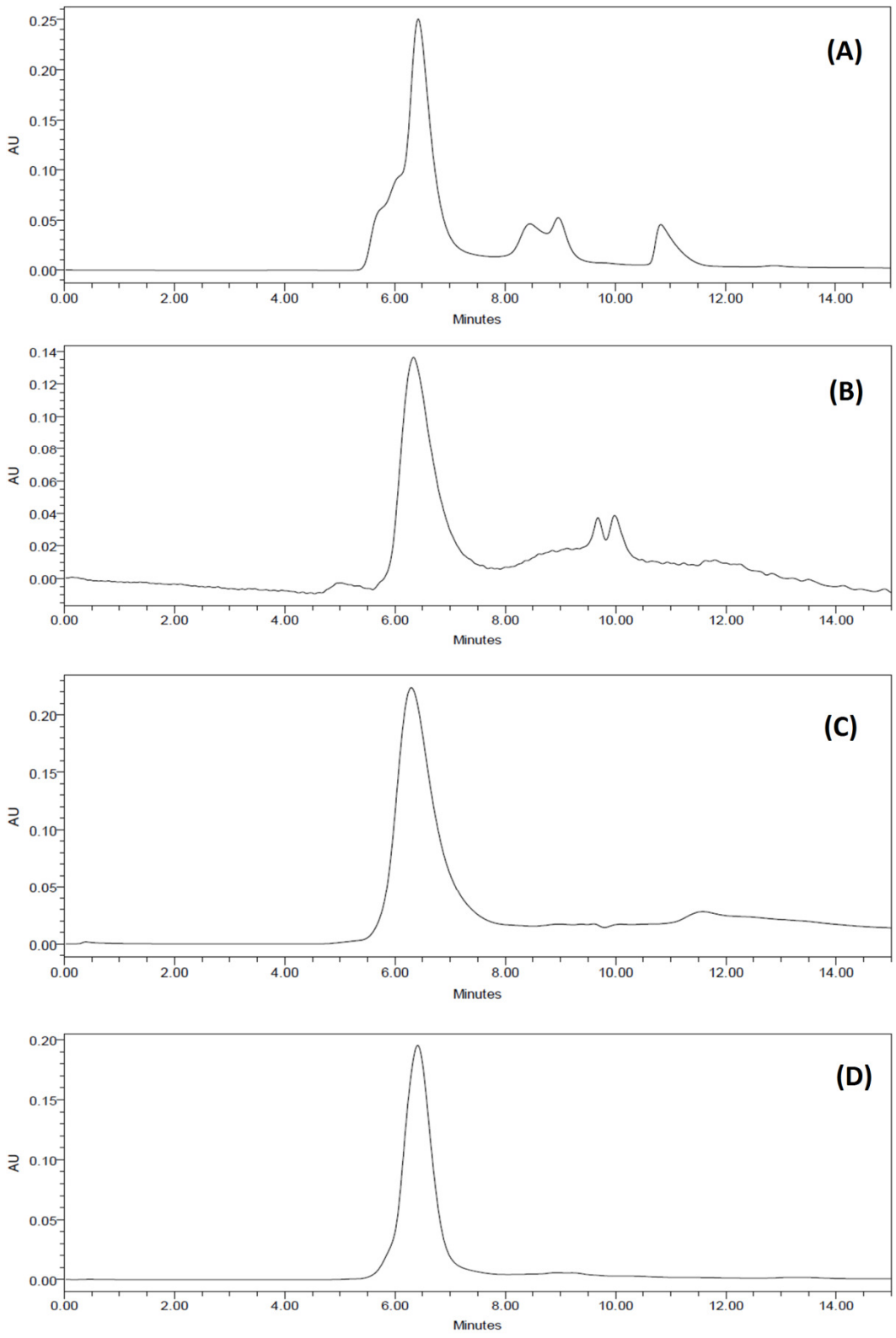

SUPPLEMENTARY FIGURE S1: Gel Permeation Chromatography profile of (A) crude rapeseed protein after dialysis, (B) clear soluble protein obtained after freeze-thaw separation, (C) 66 kDa fraction extracted from clear soluble protein, (D) Pure Bovine serum protein (molecular wt=66 kDa) standard (Sigma-Aldrich, USA) for comparison.

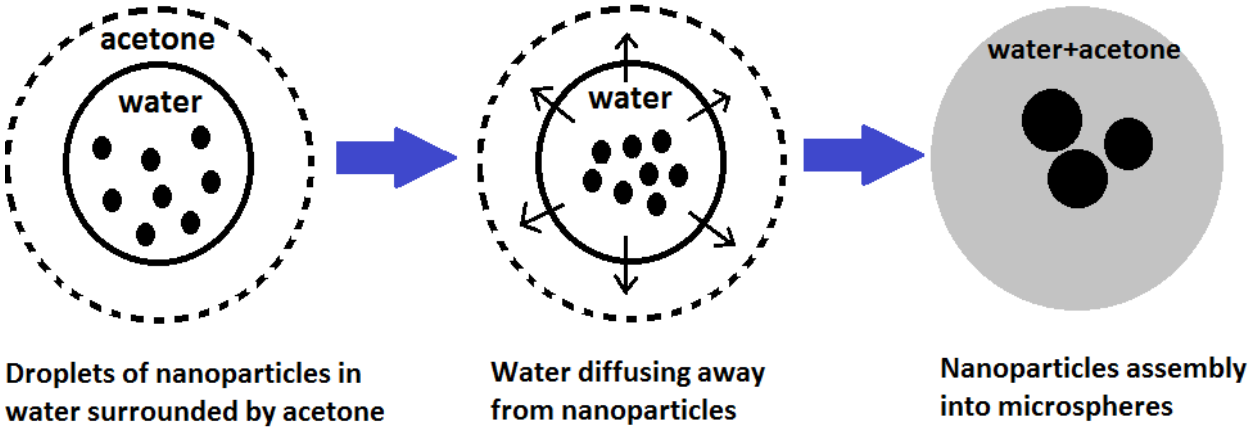

SUPPLEMENTARY FIGURE S2: Schematic presentation of formation mechanism of microspheres from CNP (Small black dot represents CNP and larger one symbolizes MS)

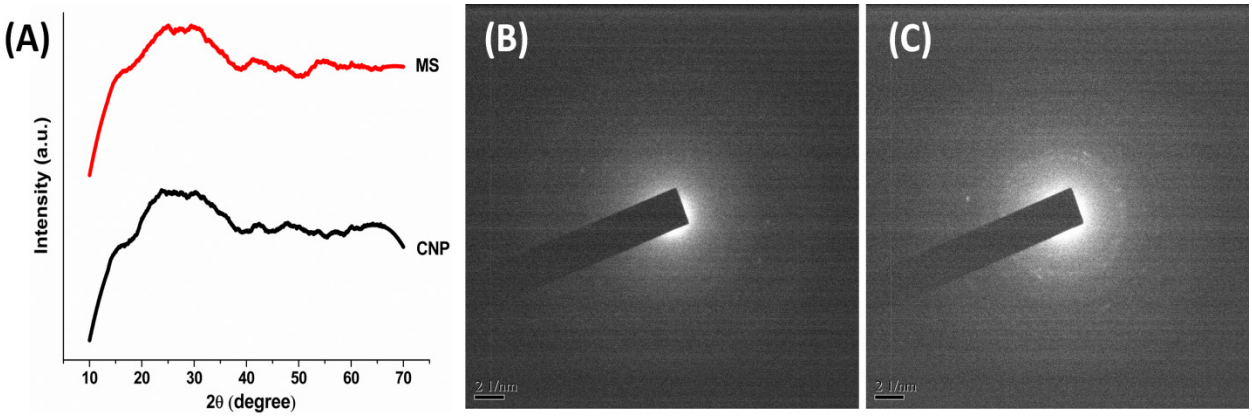

SUPPLEMENTARY FIGURE S3: (A) XRD profile of CNP and MS, and SAED pattern of (B) CNP and (C) MS.

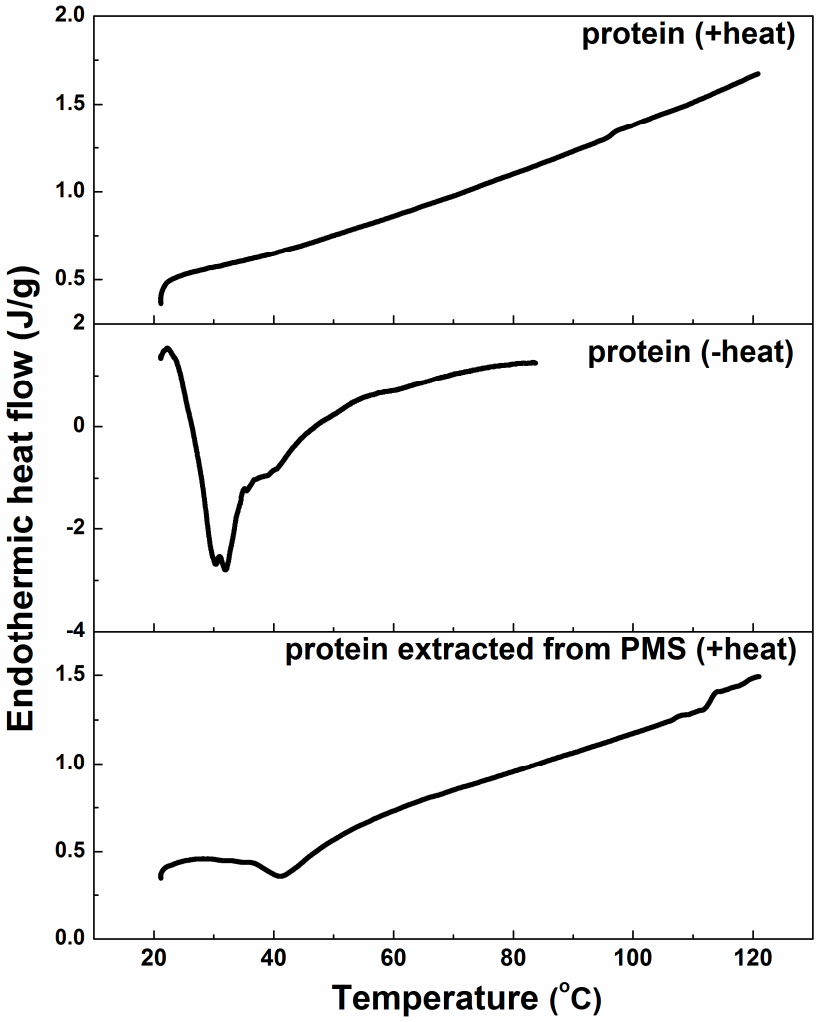

SUPPLEMENTARY FIGURE S4: DSC profile of pristine freeze-dried protein (before and after heating) and that extracted from PMS after heating.

SUPPLEMENTARY TABLE S1: Diameter of inhibition zone and Minimal Inhibitory Concentration (MIC) of CNP for various microbial strains

Strains	Positive Control (mm)	CNP (mm)	MIC (µg/mL) CNP	MIC (µg/mL) Positive Control
S. aureus (MTCC 3160)	23±0.5	30±0.3	31	1
P. duminita (MTCC 3361)	20±0.6	27±0.5	15	0.5
Y. enterocolitica (MTCC 859)	21±0.6	28±0.4	15	0.5
S. enterica typhimurium (MTCC 1252)	27±0.8	36±0.2	15	0.5
B. cereus AMDK1 (KC683896)	20±0.4	24±0.6	31	1
L. monocytogenes AMDK2 (KF894986)	29±0.5	26±0.5	31	1
M. smegmatis (ATCC 14468)	23±0.3	16±0.9	62	2
K. pneumoniae (MTCC 618)	25±0.6	29±0.8	7	0.25
C. albicans (MTCC 183)	12±1.0	27±0.6	31	2
E. coli (MTCC 40)	24±0.4	30±0.7	7	1

Each value is the mean of three replicates ± standard deviation. Gentamicin sulphate (2mg/mL) as an antibacterial and Nystatin (5mg/mL) as an antifungal agents were used as positive control.

Effect of CNP concentration on the size of MS

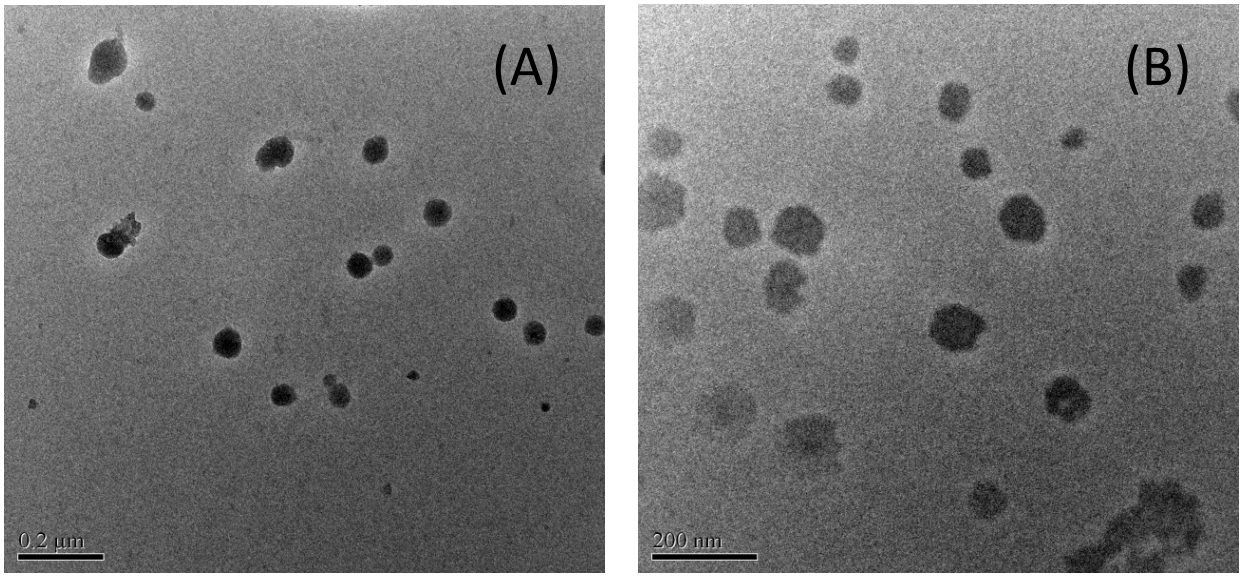

SUPPLEMENTARY FIGURE S5: Formation of MS at CNP concentration of (A) 0.1mg/mL, (B) 0.5 mg/mL

To evaluate the nanoparticle precipitation step, we examined how CNP concentration affects MS size. CNP concentrations of 0.1, 0.5 and 1 mg/mL were added with acetone (CNP solution:acetone = 1:6 v/v). We found that as the concentration decreased, the maximum sphere size also decreased. At 0.1 mg/mL, diameter of most of the spheres was ~57.54 nm (Supplementary Figure S5(A)), whereas at 0.5 mg/mL, it increased to ~109.69 nm (Supplementary Figure S5(B)), and at 1 mg/mL, the diameter further increased to ~266 nm, which is shown in main text. We propose that since the less concentrated nanoparticles solution has fewer nanoparticles, it makes smaller spheres.

Pickering emulsion preparation with CNP

Aqueous dispersion of CNP (0.2%) was used for the emulsion preparation. Rapeseed oil was added to CNP solution (oil:water = 3:7), and the system was emulsified in a water-bath sonicator (Labotec Inc., UK) for 1 h. The oil-in-water emulsion was kept for 7 days at room temperature to study the stability against phase separation, during which the emulsion droplets were viewed under TEM by flash-freezing the sample with liquid nitrogen.

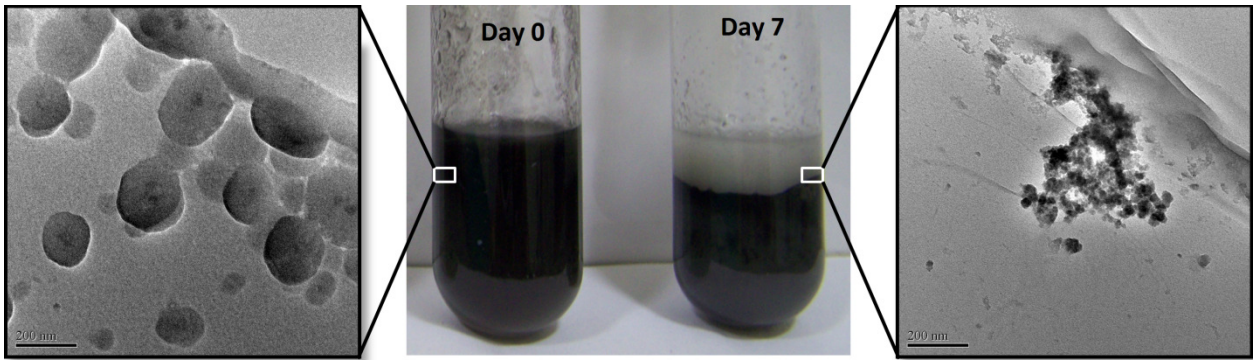

SUPPLEMENTARY FIGURE S6: Oil-in-water emulsion formed by CNP at different days of storage

TEM image (Fig S6) indicates the presence of a droplet-type emulsion surface. The uniform dark appearance of the sample indicates that the freshly formed emulsion was stable and homogeneous. Graphene oxide nanoplatelets have also been shown to stabilize oil-in-water emulsion [1], which was attributed to the electrostatic repulsion between the oil droplets coated with the highly charged graphene oxides. This might be the possible explanation for the stable emulsion observed in the present study. Furthermore, individual or aggregated CNPs can be observed within the droplets. After 7 days of storage, the separation of the two phases was clearly observable. CNP, being soluble in water, moved into the lower aqueous phase. Destabilization of the emulsion can be due to flocculation and coalescence, causing phase separation (as apparent from TEM image). The ability to form and stabilize emulsions with CNP may offer additional opportunities. Due to its antimicrobial property and dose-dependent hemocompatibility, low concentration of CNP may also hold promise for the use in emulsion-based functional foods, pharmaceutical or cosmetic formulations.

Optimization of carbon nanoparticle (CNP) synthesis parameters from oil-and-protein spent meal using Response Surface Methodology (RSM)

Oil-and-protein spent meal was dispersed in Milli-Q water such that water:meal ratio is 100:1 (v/w). Then the suspension was refluxed in an oil-bath under magnetic stirring, at each of the indicated temperature and heating duration mentioned in the design matrix. After the reaction is over, the resultant black solution was allowed to cool down and centrifuged at 3000 rpm for 10 min to separate out the unreacted residue. The brownish supernatant was dialyzed against water (using 1 kDa membrane, Himedia, India), and finally dried under vacuum at 40^{o}C to obtain CNP, whose weight is recorded.

Applying RSM with a $(2)^2$-central composite design (CCD), hydrothermal carbonization (HTC) was optimized with 2 combinations of independent variables, namely time (X_1) and temperature (X_2). The yield of CNP (Y) was considered as the response. The selected variables were coded at five levels (−1.414, 1, 0, 1, and +1.414) (Supplementary Table S2), and their real values were chosen based on preliminary experiments. The variables were coded according to the following equation:

$$x_i = \frac{X_i - X_0}{\Delta X_i} \quad (1)$$

where x_i is the dimensionless coded value of an independent variable, X_i is the real value of an independent variable, X_0 is the real value of an independent variable (X_i) at the center point and ΔX_i is the step change value. The system behavior towards the response was determined by a second-order polynomial equation, based on the equation below:

$$Y = \beta_0 + \sum \beta_i x_i + \sum \beta_{ii} x_i^2 + \sum \beta_{ij} x_i x_j \quad (2)$$

where *Y* is the predicted value for the response, β_0 is the offset term, β_i is the linear effect coefficient, β_{ii} is the squared effect coefficient and β_{ij} is the interaction effect. $x_i x_j$ represents the interaction between different coded values, where *i* is one parameter and *j* is other. Analysis of variance (ANOVA) was applied to assess the adequacy (by lack-of-fit test) and statistical significance of the developed model at a confidence level of 95% (transgression probability, $p<0.05$). Response surface plots were drawn for gaining a perspective on the interaction between the variables and how they influence the response, and also to find the optimum condition.

SUPPLEMENTARY TABLE S2: Independent variables and their levels for production of CNP from spent meal by HTC process

Independent variables	**Symbols**	**Range and levels**				
		-1.414	**-1**	**0**	**+1**	**+1.414**
Time (h)	X_1	3.172	4	6	8	8.828
Temperature (^{o}C)	X_2	131.72	140	160	180	188.28

The complete $(2)^2$-CCD design matrix consists of 13 experimental runs, including five replications at the center points (0, 0, 0) to estimate the pure experimental error, is summarized in Supplementary Table S3. The regression equation of the generated model describing the yield (Y) as a function of the uncoded factor levels, is shown in Eq. 3.

$$Y = 166.01 + 7.21X_1 + 6.96X_2 - 44.53X_1^2 - 22.98X_2^2 + 41.67X_1X_2 \quad (3)$$

The high coefficient of determination, R^2=90.12% (goodness-of-fit test) advocates a good correlation between observed and predicted values, which is also evident from Supplementary Table S3. It also indicates that at least 90% of the variability in the response could be explained by the derived second-order polynomial equation (Eq. 3). Model was highly significant ($p<0.05$) and p-value for lack-of-fit test was large ($p>0.05$) (Supplementary Table S4). This in-turn ascertains the validity of the model and is adequate for predicting the response within the conditions investigated here-in.

Supplementary Figure S7(A) shows a standardized Pareto chart of the individual, quadratic and interactive effect of the chosen independent variables (X_1 and X_2) on the response (Y). The chart includes a vertical line at the critical value for p=0.05. An effect that exceeds the vertical line may be considered significant ($p<0.05$) and those which falls below this line are taken as non-significant ($p>0.05$). The need for the use of RSM during CNP synthesis is reconfirmed by the Pareto chart; linear term of either temperature or time was found to be non-significant on the yield ($p<0.05$); whereas their interaction (X_1*X_2) and quadratic terms (X_1^2 and X_2^2) had the most significant effect ($p<0.05$).

Based on the regression equation and response surface (Supplementary Figure S7(B)), the predicted optimal condition is 6.8 h of refluxing time and temperature of 171°C. To verify the predicted values, additional experiments were conducted at the said optimum condition. The predicted yield at the optimum condition was 168.32 mg/g dry meal and the real value obtained by experimentation was found to be 170.33±1.4 mg/g dry meal. The closeness between the experimental and predicted values indicates the suitability of the model for prediction and the optimally extracted CNPs were used for further characterization.

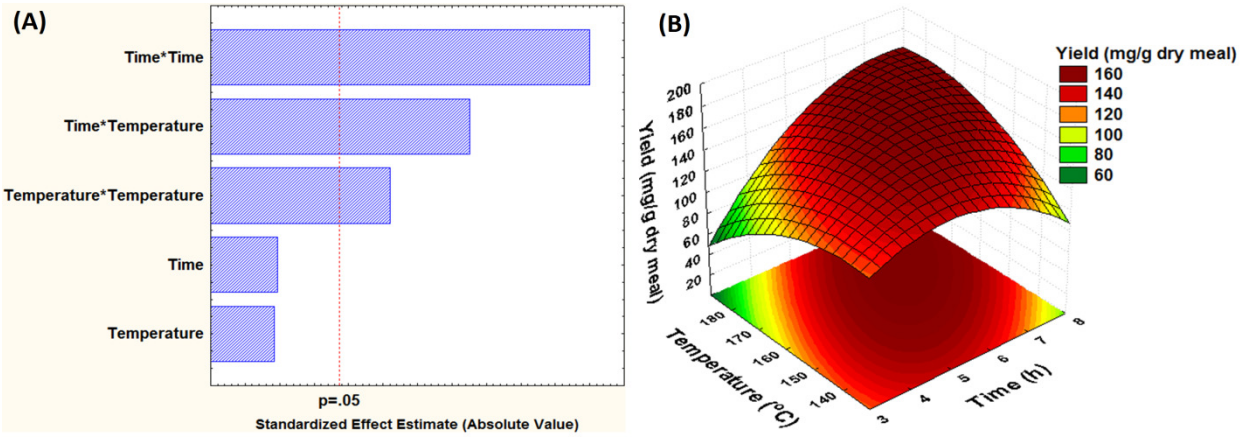

SUPPLEMENTARY FIGURE S7: (A) Standardized Pareto chart and (B) 3D response surface plot of RSM

SUPPLEMENTARY TABLE S3: Central composite design and response (dependent variable) for CNP production from spent meal by HTC

Run no.	Coded levels of independent variable		Response (Y)	
	X_1	X_2	Actual[§]	Predicted
Factorial points				
1	-1	-1	135.10±0.63[a]	143.08
2	+1	-1	116.24±0.92[b]	111.60
3	-1	+1	112.12±1.11[b]	111.25
4	+1	+1	176.60±0.27[cd]	163.11
Axial points				
5	-1.414	0	120.45±0.53[b]	114.28
6	+1.414	0	117.01±1.89[b]	128.69
7	0	-1.414	139.58±0.36[a]	136.08
8	0	+1.414	140.97±0.71[a]	149.99
Center points				
9	0	0	161.72±0.82[c]	166.01
10	0	0	164.80±0.45[c]	166.01
11	0	0	159.83±1.22[c]	166.01
12	0	0	169.98±0.93[c]	166.01
13	0	0	173.74±1.64[d]	166.01

[§]Values are means±standard deviation of n=3 analyses (subjected to Tukey test). Means with the same letter within one column were not statistically different (p>0.05).

SUPPLEMENTARY TABLE S4: ANOVA of regression model built for CNP yield (response)

Source	DF	Seq SS	Adj SS	Adj MS	F	*p*
Regression	5	6107.6	6107.6	1221.52	12.77	0.002
Linear	2	401.1	401.1	200.57	2.10	0.193
Square	2	3970.1	3970.1	1985.04	20.75	0.001
Interaction	1	1736.4	1736.4	1736.39	18.15	0.004
Residual Error	7	669.7	669.7	95.67		
Lack-of-Fit	3	536.1	536.1	178.71	5.35	0.069
Pure Error	4	133.6	133.6	33.39		
Total	12	6777.3				

SS, sum of squares; *df*, degree of freedom; MS, mean squares; *p*, transgression probability

The effect of time and temperature on nanoparticle morphology is shown below. In all tested conditions, spherical particles of nanometer scale were obtained. However, synthetic products formed at lower temperature (especially at 132 and 140^{o}C) resembled with entangled fibers. Carbon fibres with different shapes may be obtained at a lower temperature [2]. Likewise, Sevilla and Fuertes [3] observed graphitic carbon nano-structures with coil morphology from cellulose. Thus, it is proved that rapeseed spent meal can act as excellent precursor for the preparation of nanoscale products.

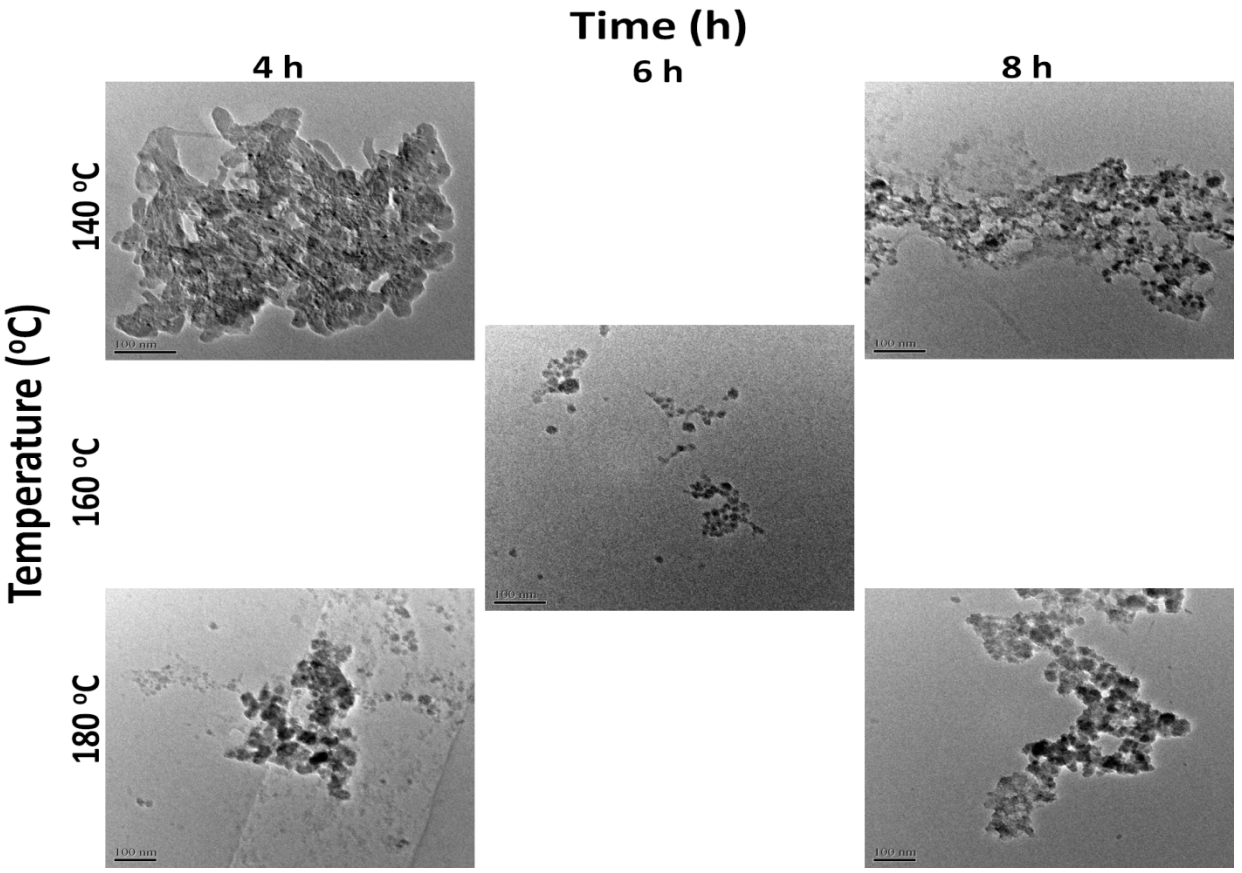
Time (h)
4 h
6 h
8 h
Temperature (°C)
140 °C
160 °C
180 °C
100 nm

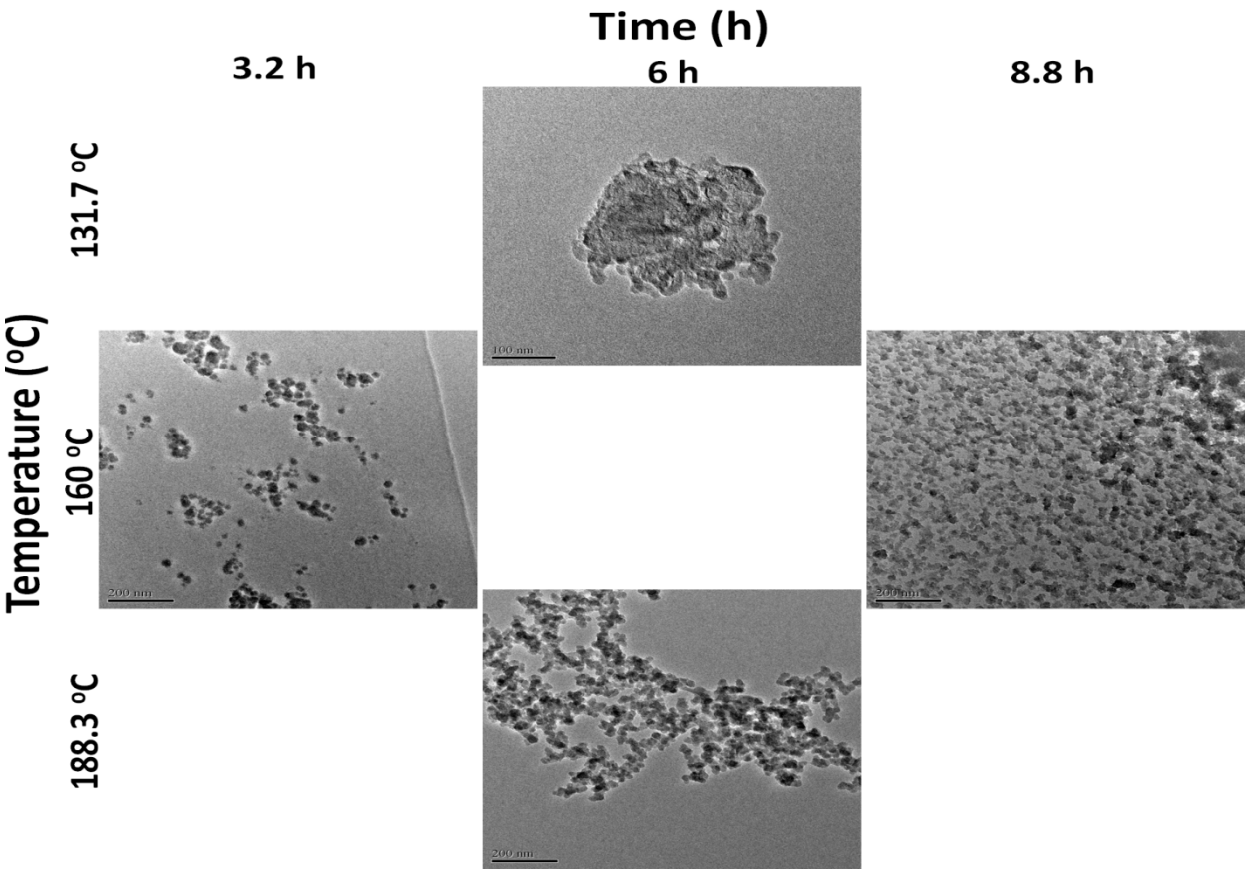
Time (h)
3.2 h
6 h
8.8 h
Temperature (°C)
131.7 °C
160 °C
188.3 °C
100 nm
200 nm

Supplementary References

[1] K. Y. Yoon, S. J. An, Y. Chen, J. H. Lee, S. L. Bryant, R. S. Ruoff, C. Huh, and K. P. Johnston, "Graphene oxide nanoplatelet dispersions in concentrated NaCl and stabilization of oil/water emulsions," *Journal of Colloid and Interface Science*, vol. 403, pp. 1-6, 2013.

[2] X. X. Zhang, Z. Q. Li, G. H. Wen, K. K. Fung, J. Chen, and Y. Li, "Microstructure and growth of bamboo-shaped carbon nanotubes," *Chemical Physics Letters*, vol. 333, pp. 509-514, 2001.

[3] M. Sevilla and A. B. Fuertes, "Graphitic carbon nanostructures from cellulose," *Chemical Physics Letters*, vol. 490, pp. 63–68, 2010.

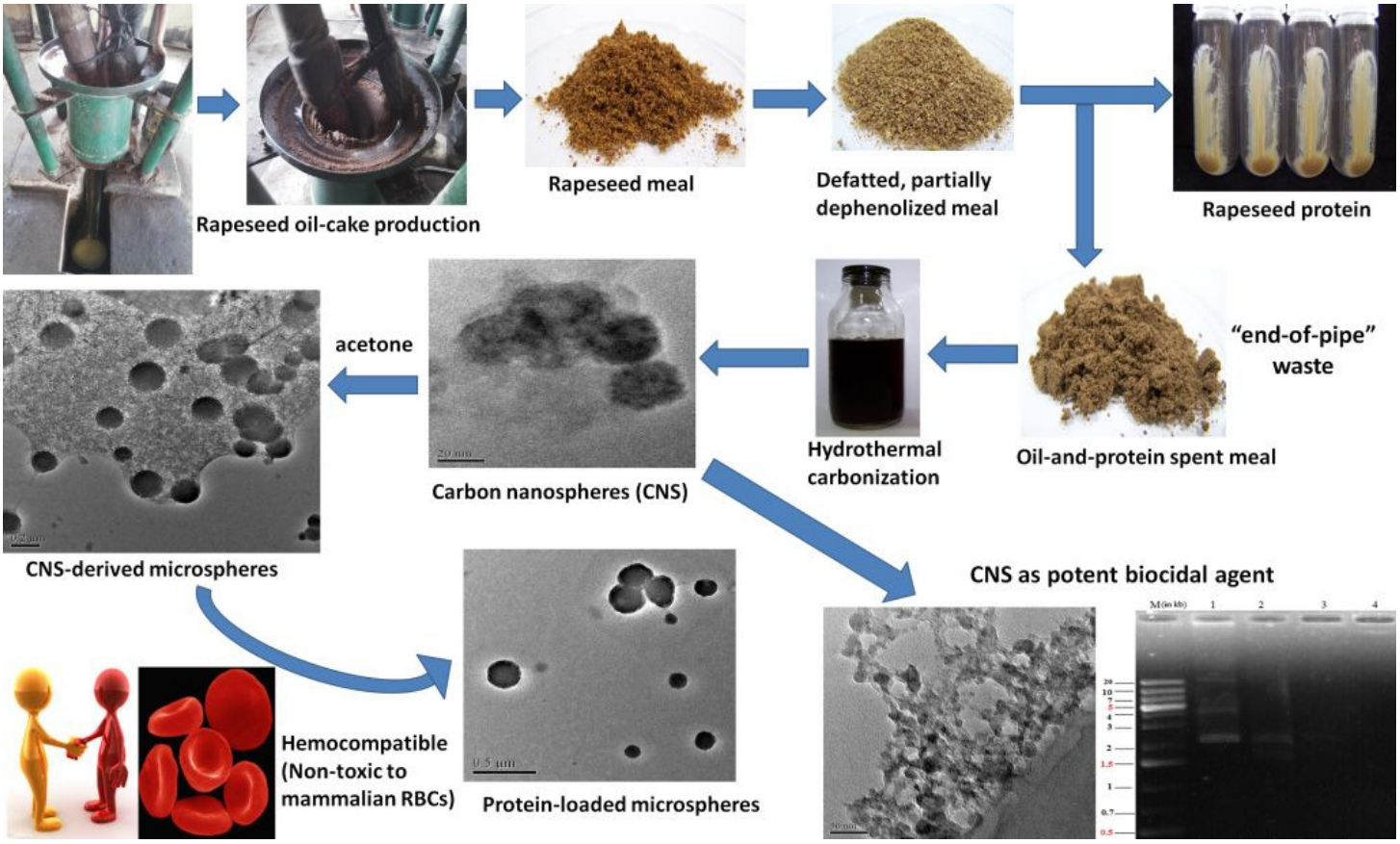

Summarization of the work